International Journal Of Engineering Research And Development
e- ISSN: 2278-067X, p-ISSN: 2278-800X, www.ijerd.com
Volume 20, Issue 3 (March. 2024), PP. 250-264

Design and Performance Analysis of Massive MIMO Antenna for Sub-6 GHz 5G Applications

Micah A. Okon[1], Akaninyene Obot[2], Kufre Udofia[3], Jimoh Afolayan[4]
[1,2,3,4]*Department of Electrical and Electronics Engineering, Faculty of Engineering*
University of Uyo, Uyo, Akwa Ibom State, NIGERIA

ABSTRACT
This paper explored the critical aspects of Massive Multiple Input Multiple Output (mMIMO) antenna systems tailored for 5G base station applications within the Sub-6 GHz frequency range. A comprehensive performance analysis, evaluating key parameters such as s-parameters, gain, beamwidth, radiation characteristics, envelop correlation coefficient (ECC), and diversity gain (DG) was done. The proposed antennas performed admirably well with improved gain (over 6 dB per element in the case of the 40-element MIMO antenna and over 9 dB for each antenna element of the 84-element mMIMO antenna), consistent impedance bandwidth, impulse reception characteristics (evidenced by VSWR: 1≤VSWR≤2), high radiation efficiency, nearly omnidirectional radiation pattern on the average. The perceived drawback of size counts for little, considering the prescribed area of use. The outcomes of this research contribute valuable insights into the optimal design and performance attributes of mMIMO antennas, offering practical guidance for engineers and researchers involved in the deployment and advancement of 5G networks. The findings are anticipated to inform the ongoing development of 5G infrastructure, facilitating the realisation of efficient and high-capacity wireless communication systems for diverse applications in the Sub-6 GHz frequency band.
Keywords: *mMIMO, fifth-generation, sub-6 GHz, base station, analysis.*

Date of Submission: 13-03-2024 Date of Acceptance: 27-03-2024

I. INTRODUCTION

According to Bhatia and Kunte (2019) and Kuboye (2018), the multiuser problem has been a significant challenge faced by the LTE standard from inception since many User Equipment (UE) in the same geographical location require high data rates in a finite bandwidth with low latency. Due to the finite bandwidth available for multiple users, resource allocation method was employed to manage individual UE requests and improve quality of service (QoS) within the LTE Base Station (BS) referred to as eNodeB. This resource management technique equally reached its limit, with engineers and scientists having to shift focus to upper-frequency bands where more bandwidth was readily available, hence the choice of deployment of fifth-generation (5G) of mobile communication at the millimetre wave (mmWave) frequency band mainly for the purpose of achieving higher data throughput realisation.

Furthermore, as mobile/wireless communication has grown to become almost a default means of reaching thousands (and even millions) per time, lower frequency bands have become too congested for newer technology deployment. As was captured by Yussuff and Khamis (2012), more bandwidth is made available with increasing frequency (carrier frequency), which was the motivation behind the standardisation of 5G and beyond technologies. Conversely, as the transmitting frequency goes up, the optimal radiating size of the antenna element comes down. Simply put, as the frequency of operation increases, antenna size reduces, which implies that power per element available for adequate signal transmission also reduces. Consequently, at every point in time, more antenna elements are required for signal transmission per time. This, as submitted by Zhao et al. (2019), was the reason behind the concept of massive MIMO in mmWave 5G.

However, due to the characteristic short wavelength associated with high-frequency signal transmission, the need for the installation of multiple picocells becomes sacrosanct to the usefulness of the deployed 5G signal, thereby increasing the overall deployment cost of the technology in general. As a result, several network operators have opted for the deployment of the 5G technology using sub-6 GHz frequencies (C-band 5G) so as to achieve broader signal coverage per macrocell and also act as cost-saving measures.

In this paper, the design and performance analysis of massive MIMO antenna system for sub-6 GHz 5G application is proposed. The antenna was designed to operate at a frequency of 3.6 GHz in a cluster pair of 8 x 2 array arrangement. Analysis of the designed antenna was done after simulation in Computer Simulation Studio (CST Studio). Fundamental antenna parameters such as return loss, antenna gain, diversity gain, and envelope correlation coefficient (ECC) aided the performance assessment of the proposed antenna. This paper is

arranged sections as follows: section 1 is the introduction to the study; some related articles are reviewed in section 2 and the design methodology is presented in section 3. Results achieved are summarized in section 4 which is briefly followed by a conclusion with references appended thereafter.

II. REVIEW OF SOME RELATED LITERATURE

The likes of Abedian et al. (2017), Al-Ajrawi and Rahhal (2015), Jamshed et al. (2021), Kim and Kim (2021) Li et al. (2018), Nithya et al. (2021), Sandi et al. (2022), Yang et al. (2021); have worked on MIMO antennas however, a few of them are examined in detail in this section.

Ref (Nithya et al., 2021) proposed a wide band eight-element MIMO array with high element isolation enrichment for 5G metal frame smartphones. The authors first designed a single-band rectangular microstrip antenna on an Epoxy FR4 substrate with a dielectric constant of 4.4, which was doubled in a 2×1 configuration and then finally converted to a 4×2 array configuration. The antenna resonated at 3.9, 4.5, and 5.8 GHz, respectively. Their design objectives to measure the yardstick for attainment were not clearly defined.

Al-Ajrawi and Rahhal (2015) proposed the design of a mMIMO antenna using an inset-fed rectangular microstrip antenna as the primary element at 1.5 GHz on a Rogers Ultralam 1217 (tm) substrate material. The antenna comprised a 2×33 arrangement with better antenna characteristics in comparison to the single-band antennas. However, despite the number of elements that constituted their proposed mMIMO antenna, the realised gain was not a significant improvement over the single-band antenna gain.

In their paper, Sandi et al. (2022) proposed a design to improve isolation between antenna elements and enhance the performance of mMIMO antennas. They adopted a combination of dielectric resonators, electromagnetic bandgap (EBG), and defected ground structure (DGS) techniques at a 5G frequency band of 3.5 GHz. The substrate material used was FR-4 with a dielectric constant (εr) of 4.3. Results from simulation and measurements showed an improvement in mutual coupling, widening of bandwidth, and increased antenna gain. The range of frequency covered by their proposed antenna is different from what is presented in this study.

Al-Tarifi et al. (2018) presented the design and analysis of a 72 port (288 antennas) triangular-shaped mMIMO antenna system for 5G base stations. Each side of their proposed antenna system comprised three (3) layers occupying a footprint of $44.4 \times 29.6 \times 0.1524\ cm^3$, and contained 24 ports in total. Each port (subarray) consisted of 2×2 patches on the top layer; their feed network with pre-calculated phases is on the bottom layer, and the ground plane constituted the middle layer. Resonation of their proposed antenna was realised in dual operating modes. The first mode was an individual port MIMO mode with low correlation between different ports for high signal-to-noise-ratio (SNR) scenarios (each subarray was operating independently and had beams directed away from its adjacent elements). The second mode comprised an array beam switching for lower SNR scenarios that provided dedicated beams for users. Though their antenna presented achieved significant antenna gain, it was hampered by limited bandwidth (100 MHz).

III. METHODOLOGY

Single-band rectangular microstrip antenna (RMSA) with 3.6 GHz centre frequency on a Roger RT Duroid substrate with a dielectric constant (ε_r) of 2.2 and height (h) of 1.6 mm was designed, simulated, and finetuned after analysis. This antenna formed the basis on which the number of elements was increased in pairs to achieve the massive MIMO characteristics. A dual patch antenna arrangement was used to realise sufficient signal quality for the proposed MIMO. Microstrip quarter-wave feed line was used in a series-array feeding network to interconnect each primary element to the corresponding secondary patch, thereby constituting an antenna pair to link the $50\ \Omega$ terminal of the sub-miniature version A (SMA) connector. These steps were executed in phases in order to forestall deviations from the study objectives due to coupling between antenna elements. The antenna parameters from simulated results was analysed and compared with related literature.

3.1 Survey Design

The transmission line model equations from Balanis (2016), Kumar and Ray (2003), and Huang and Boyle (2008) were used to create a single-band microstrip antenna with a centre frequency 3.6 GHz. The rectangular patch structure functions as a resonator; therefore, its length and width are commonly chosen so that, for effective and enhanced radiation, $L_P < W_P < 2L_P$. The following is a list of the precise design equations for the rectangular microstrip patch.

i) The width (W_P) of the microstrip patch antenna computed from (1).

$$W_P = \frac{c}{2f_r\sqrt{\frac{(\varepsilon_r+1)}{2}}} \quad (1)$$

ii) The effective dielectric constant (ε_{reff}) is obtained from (2).

$$\varepsilon_{reff} = \frac{\varepsilon_r+1}{2} + \frac{\varepsilon_r-1}{2}\left[1 + 12\left(\frac{h}{W_P}\right)\right]^{-1/2} \quad (2)$$

iii) The effective length L_{eff} of the patch can be derived from (3).

$$L_{eff} = \frac{c}{2f_r\sqrt{\varepsilon_{reff}}} \quad (3)$$

iv) The extension length (ΔL) is deducted from the calculated length L_P of the patch retaining the actual length of the patch unchanged. The extension length virtually appears due to the fringing field, as seen in (4):

$$\Delta L = 0.412h\frac{[\varepsilon_{reff}+0.3]\left[\frac{W}{h}+0.264\right]}{[\varepsilon_{reff}-0.258]\left[\frac{W}{h}+0.813\right]} \quad (4)$$

v) Calculation of actual length of patch (L_P): From Equation 5, the actual length of the patch (L_P) is:

$$L_{eff} = L_P + 2\Delta \quad (5)$$

$$L_P = L_{eff} - 2\Delta L$$

vi) Calculation of the ground plane dimensions (Lg and Wg): The usage of infinite ground planes is a key premise of the transmission line model. For practical considerations, a limited ground plane is necessary, nevertheless. The size of the ground plane for both finite and infinite ground planes is greater than the patch dimensions by around six times the substrate thickness all the way around Saturday et al. (2017). Consequently, the ground plane dimensions for this design are determined as follows:

$$Lg = L_P + 6h \quad (6)$$

$$Wg = W_P + 6h \quad (7)$$

vii) Determination of the patch thickness (t): The metallic patch is selected to be very thin such that:

$$t << \lambda_0 \quad (8)$$

Quarter-wave feeding technique was used for the feedline to the patch, and the design equations were adopted from (Aduke et al., 2018).

The schematic diagram and table containing computed dimensions of the 3.6 GHz patch antenna are shown in Figure 1 and Table 1, respectively, while the designed antenna in CST Studio is shown in Figure 2.

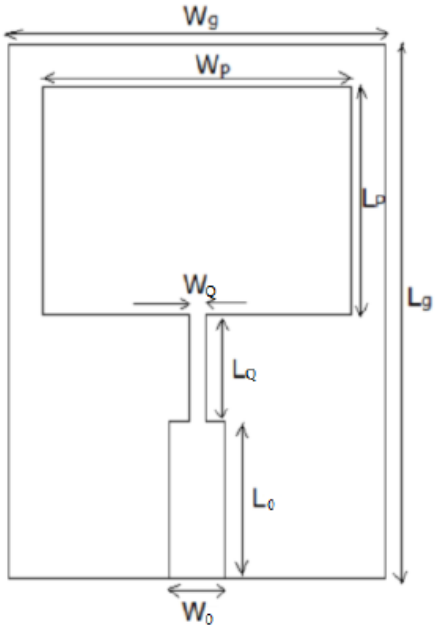

Figure 1: Schematic diagram with dimensions of the designed antenna

Table 1: Design dimensions of 3.6 GHz single band edge fed RMSA

Design Parameter	Values
Length (L_p)	27.47 mm
Width (W_p)	32.92 mm
Dielectric constant (ε_r)	2.2
Substrate height (h)	1.60 mm
Patch thickness (t)	0.035 mm
Length of ground plane (L_g)	29.82 mm
Width of ground plane (W_g)	35.68 mm
Width of quarter wave feed section (W_Q)	0.78 mm
Width of 50 Ω transmission line (W_0)	3.10 mm
Length of 50 Ω transmission line (L_0)	7.00 mm
Length of quarter wave feed line (L_Q)	15.97 mm
Input edge impedance of the patch (R_{in})	197.28 Ω
Characteristic impedance of the feed line (Z_0)	50 Ω
Characteristic impedance of quarter wave transformer (Z_1)	99.32 Ω

The designed 3.6 GHz edge-fed RMSA in CST MWS Studio is shown in Figure 2.

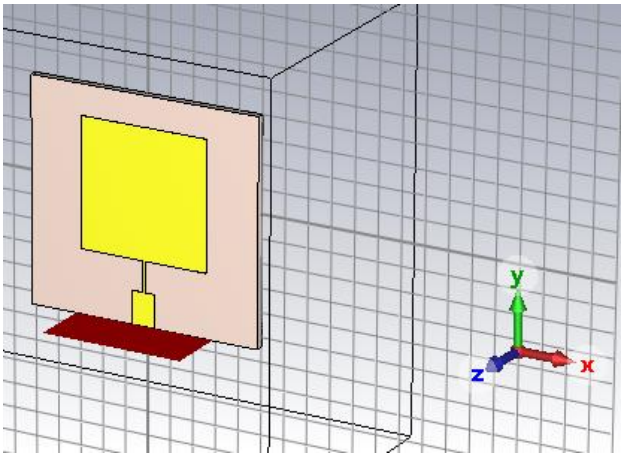

Figure 1: Designed antenna using CST MWS Studio

Variants of the geometry in Figure 1 were also studied to ascertain their characteristics; these are presented in detail in the subsections.

3.2 Design of Massive MIMO Antenna

In combining multiple elements on a single substrate, the challenge of mutual coupling of antenna elements arises due to the simultaneous reflections at similar frequencies (Chen et al., 2018). However, Garg et al. (2001) posited that in order to lower the risk of mutual coupling, maintain single-mode propagation among radiating elements, and have in-phase element characteristics as well as radiation in normal direction, the distance between elements is approximated to be about half wavelength $\left(\frac{\lambda_{air}}{2}\right)$; thus, patch spacing, $d = \frac{\lambda_{air}}{2}$.

Ref (Saurabh et al., 2020) proposed the orthogonal placement of antenna elements to achieve high isolation. This idea informed how antenna elements were placed on the proposed MIMO antenna layout, and this was done incrementally till the 84-element mMIMO antenna was realised. The dimensions of the substrate for the various antenna configurations are highlighted in Table 2. Figures 3 and 4 show the design of 2×1 and 2×2 laterally inverted antenna elements in CST studio.

Table 2: Substrate dimensions of proposed multi-element antenna

Antenna Configuration	Substrate Dimension
2×1 antenna	$50\ mm \times 107\ mm$
2×2 antenna	$100\ mm \times 107\ mm$
40-element MIMO	$1001.50\ mm \times 107\ mm$
84-element massive MIMO	$1001.50\ mm \times 267\ mm$

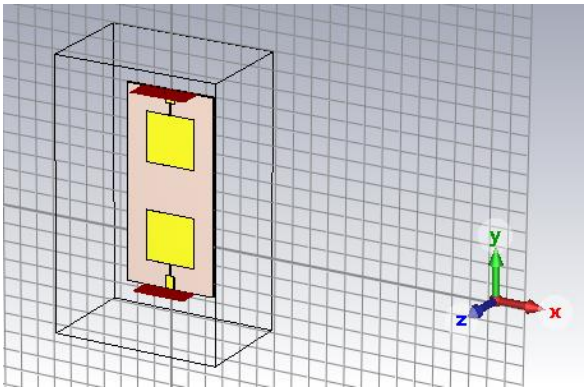

Figure 3: Designed 2×1 MIMO antenna using CST studio

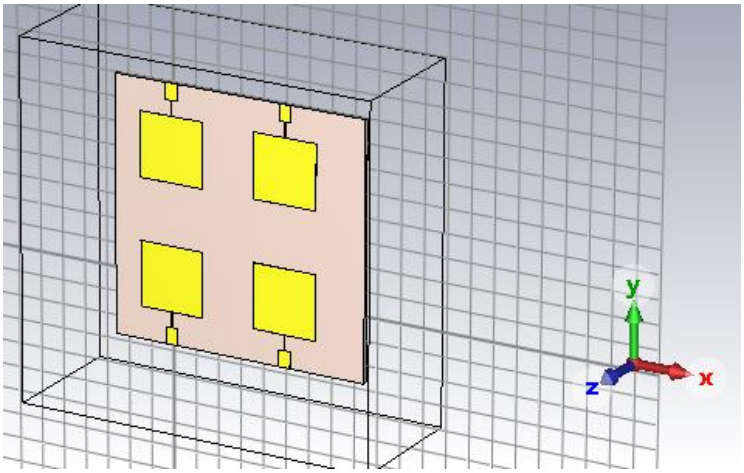

Figure 4: Designed 2×2 MIMO antenna using CST studio

The 40-element MIMO investigated in this study is presented in Figure 5.

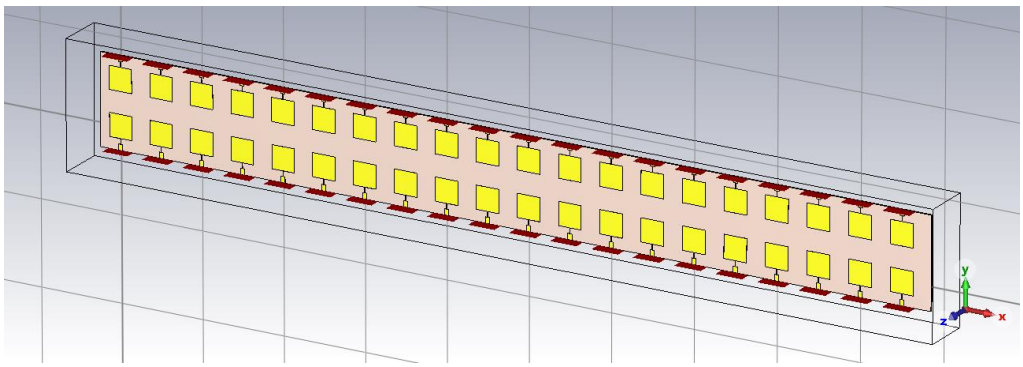

Figure 5: Proposed 40-element mMIMO antenna designed in CST Studio

Furthermore, (Wang et al., 2017) proposed a series-fed microstrip antenna array configuration from which the idea for the antennas presented in Figures 6 and 7 were derived. Also, a rule of thumb suggested by Singh and Gupta (2013) and Kumar and Gupta (2013) is that since a 50 Ω rated line feeds the microstrip patch, the feed

line emanating from the feeding patch should equally maintain the same width transformed from the previously used quarter-wave line for the receiving patch.

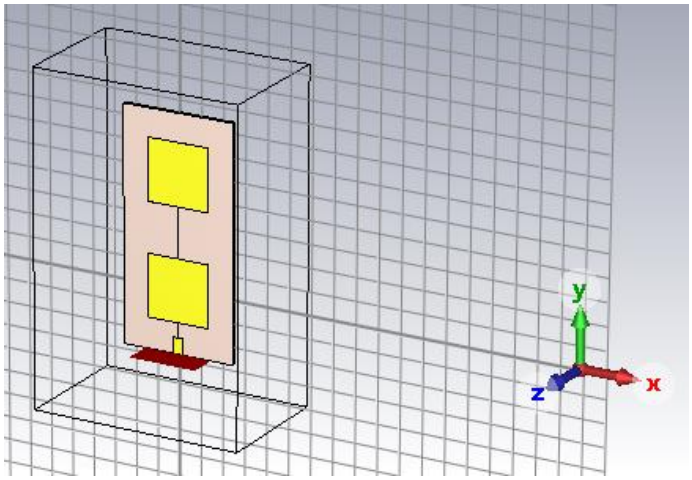

Figure 6: Designed 2 × 1 series-fed antenna using CST studio

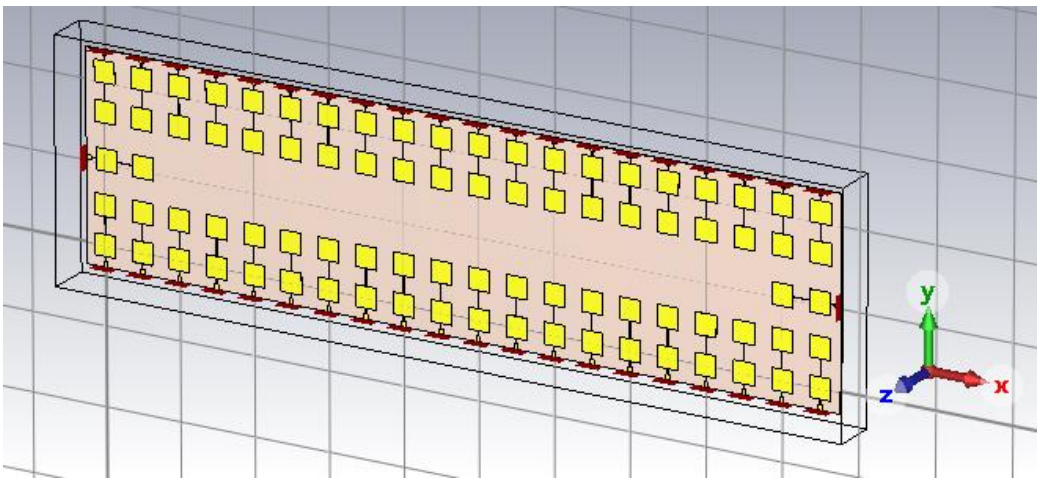

Figure 7: Proposed 84-element mMIMO antenna designed in CST Studio

IV. RESULTS

Six antennas, including a quarter-wave-fed single band antenna, a 2 × 1 MIMO antenna, a 2 × 1 series-fed array antenna, a 2 × 2 MIMO antenna, a 40-element MIMO antenna, and a series-fed 84-element mMIMO antenna array, have been designed at 3.6 GHz for telecommunication base station application in the preceding section. This section presents the results and performance analysis of every antenna design in Section 3. Both 2-D and 3-D versions of the results are presented (3-D). Every plot depicted in this section is the simulation result from CST MW Studio, showing antenna parameters, such as return loss, VSWR, directivity, antenna gain, diversity gain, envelop correlation function, and current distribution pattern around the antenna.

4.1 Return Loss Plots and Impedance Bandwidth of Designed Antennas

Figure 8 shows a minimum return loss of -13.9439 dB at a resonant frequency of 3.6 GHz for the single-band QWT-fed RMSA antenna. As observed from Figure 8, a bandwidth of 62.71 MHz was achieved. Similarly, at 3.6 GHz, the minimum return loss (S_{11}) of -11.6706 dB and minimum return loss (S_{22}) of -11.3684 dB was achieved with bandwidths of 72.33 MHz and 67.81 MHz by the 2 × 1 QWT-fed MIMO antenna, as given in Figure 9.

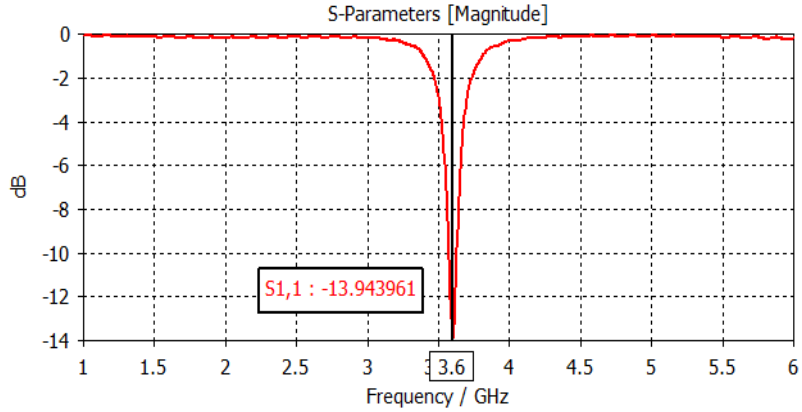

Figure 8: Return Loss plot of the quarter-wave-fed single-band antenna at 3.6 GHz

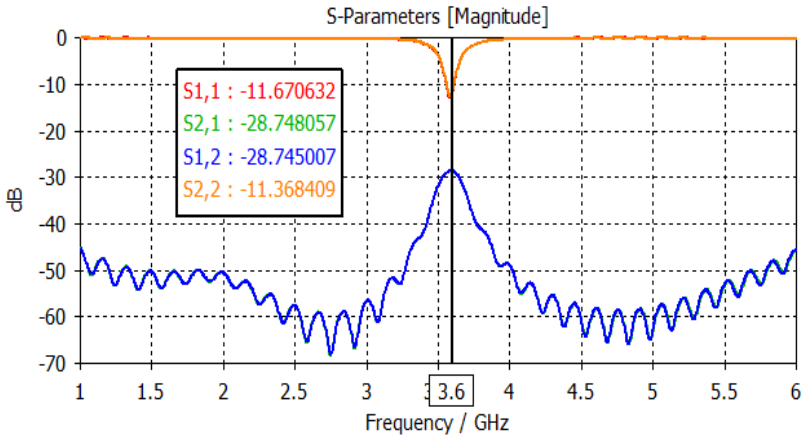

Figure 9: Return Loss plot of 2 × 1 MIMO antenna at 3.6 GHz

Minimum return loss (S_{11}) of -13.176 dB was achieved with a bandwidth of 60.77 MHz by the 2 × 2 MIMO antenna, as illustrated in Figure 10. Similar characteristics are observed on the return loss plot of the proposed 40-element MIMO antenna designed at 3.6 GHz, as shown in Figure 11.

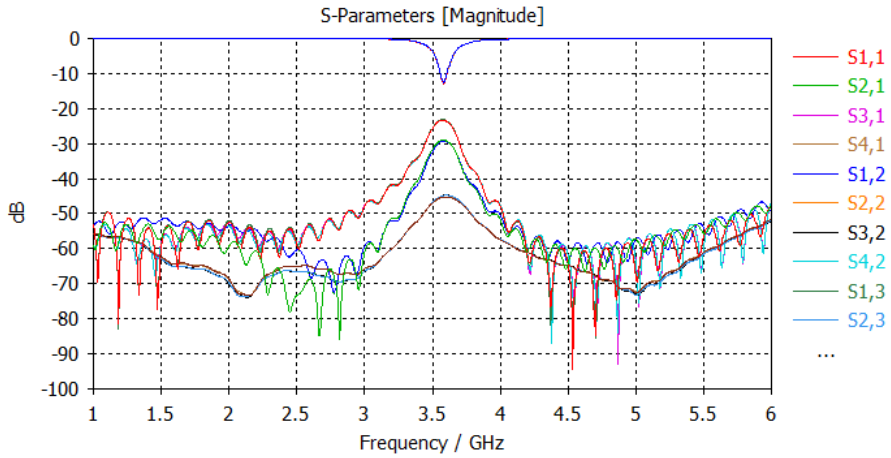

Figure 10: Return Loss plot of 2 × 2 MIMO antenna at 3.6 GHz

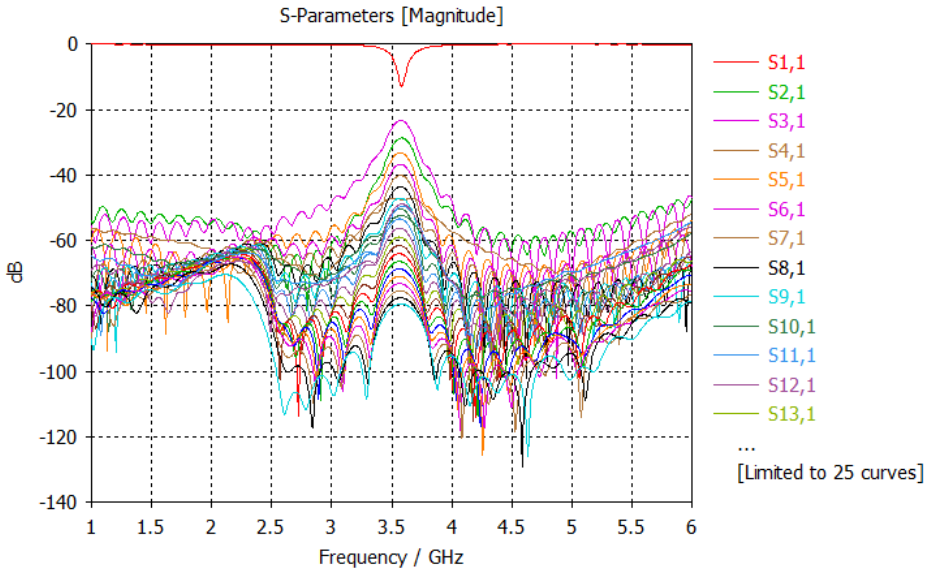

Figure 11: Return Loss plot of 40-element MIMO antenna at 3.6 GHz

A return loss of -21.2740 dB with a bandwidth of 80.50 MHz was achieved by the series-fed 2x1 MIMO antenna, as presented in Figure 12. Similarly, the return loss plot of the 84-element mMIMO antenna with all port configurations is illustrated in Figure 13.

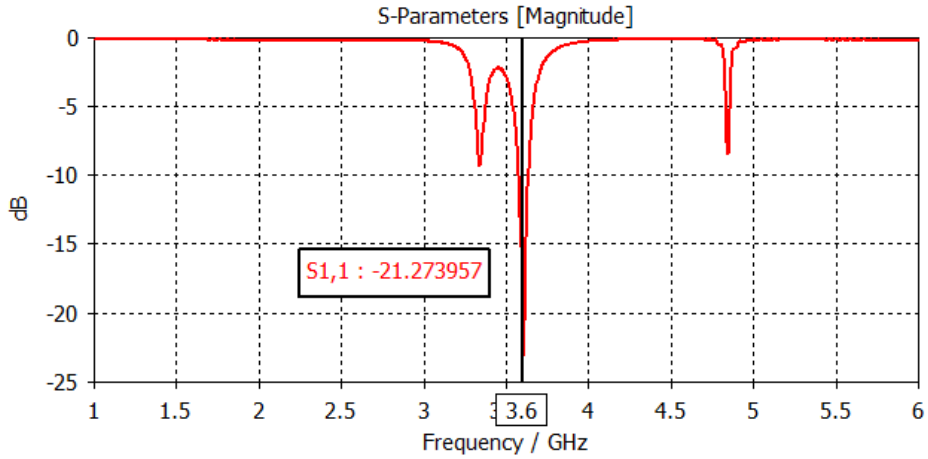

Figure 12: Return loss of 2 × 1 series-fed antenna

A noteworthy characteristic of all the multi-element antennas presented in Figures 9 to 13 is the consistently reduced mutual coupling and port isolation among resonating antenna elements. This is a desired property of all MIMO antennas, especially for application flexibility.

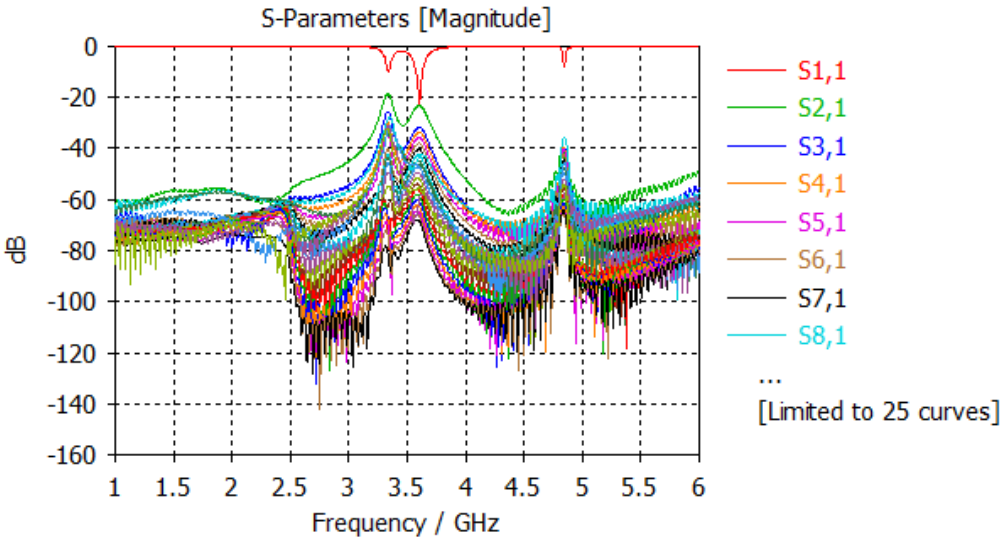

Figure 13: Return Loss plot of 84-element series-fed mMIMO antenna at 3.6 GHz

4.2 Voltage Standing Wave Ratio (VSWR) and Gain of the Designed Antenna

The VSWR plot of the proposed antennas at 3.6 GHz measured at points of minimum return loss is illustrated in Figures 14 and 15.

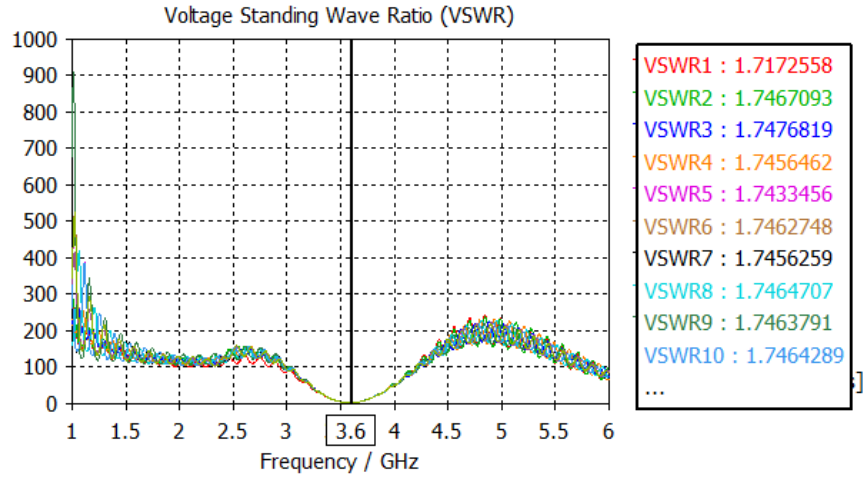

Figure 14: VSWR of the 40-element mMIMO antenna 3.6 GHz

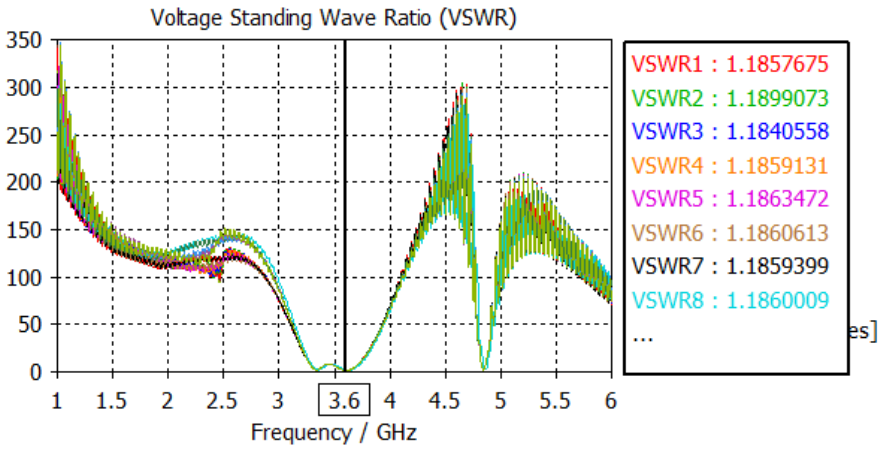

Figure 15: VSWR of the proposed 84-element series-fed mMIMO antenna at 3.6 GHz

The results show that the antennas resonated within the prescribed limits of $1 < VSWR < 2$. On average, a VSWR value of 1.74 and 1.19 was achieved by all the elements of the 40-element MIMO antenna and 84-element mMIMO antenna, as shown in Figures 14 and 15.

4.3 Envelop Correlation Coefficient (ECC) and Diversity Gain (DG)

For an acceptable MIMO performance, channel capacity losses (CCL) and envelop correlation coefficient (ECC) should be less than 0.5, while the total active reflection coefficient (TARC) should be below 0 dB Amin et al. (2019). Figure 16 gives the proposed ECC plot of the MIMO antennas. The ECC achieved at design frequencies for the proposed 2×2 MIMO antenna shows compliance with < 0.5 standard.

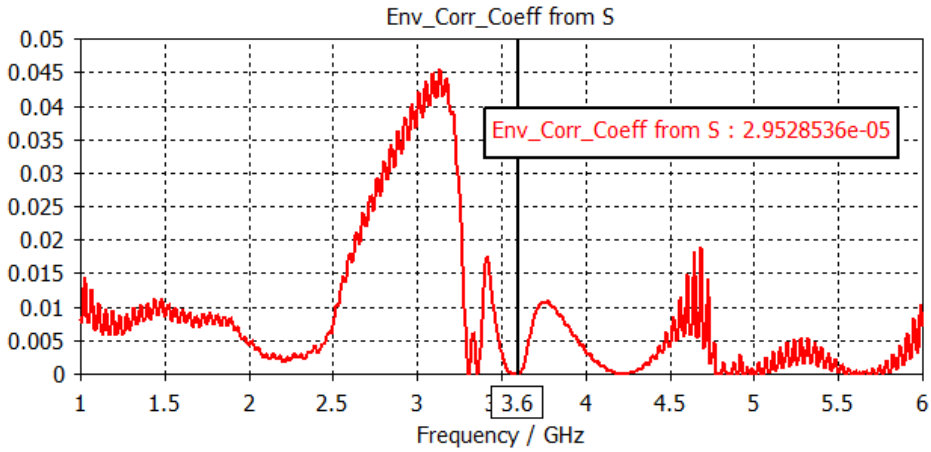

Figure 16: ECC of 2×2 MIMO antenna

The diversity gain is computed according to the formula given by Dkiouak et al. (2019) in (9).

$$DG = 10\sqrt{(1 - |\rho|^2)} \tag{9}$$

Where ρ is the complex cross-correlation coefficient and $|\rho|^2 = (ECC)^2$

From Figure 4.13, ECC at 3.6 GHz is 0.00002953, thus substituting the ECC value into Equation (9);

$$DG = 10 \times \sqrt{(1 - 0.00002953^2)}$$
$$= 10 \times \sqrt{0.999985} = 9.99985$$

The computed value agrees with the plot shown in Figure 17.

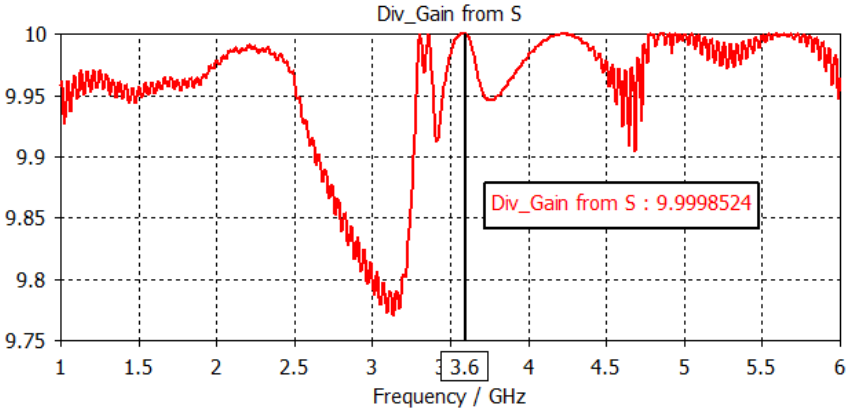

Figure 17: Diversity gain of 2×2 MIMO antenna

For the avoidance of repeated computation, the results obtained from Equation (9) and that of Figure 17 are similar for all the ports of the proposed antennas.

4.4 Gain of Proposed MIMO Antennas

In terms of antenna gain, Table 3 gives a summary of the various antenna gain achieved by the studied antennas.

Table 3: Gain (IEEE) of all designed antennas

Antenna	Gain (dB)
QWT-fed single element antenna	6.06
QWT-fed 2x1 MIMO antenna	6.48
QWT-fed 2x2 MIMO antenna	6.51
QWT-fed 40-element antenna	6.53
Series-fed 2x1 antenna	9.29
Series-fed 84-element mMIMO antenna	9.38

It is important to note that aside from the nominal antennas (single element and series-fed 2×1 antennas), only the first antenna element gain of the MIMO antennas was extracted for analysis on every other antenna.

4.5 Directivity and Radiation Pattern of Designed Antennas

The directivity plots (H-plane and E-plane) of all antennas designed in Section 3 are presented in this subsection. All proposed antenna radiation patterns are observed to be on the broadside. Figure 18 shows the H-plane ($\varphi = 90°$) directivity of the QWT-fed single patch antenna and 2×1 series-fed patch antenna at 3.6 GHz having main lobe magnitudes of 7.2 dBi and 9.84 dBi, and main lobe directions of 5^o and 4^o, respectively. Half power beamwidth (HPBW) of 78.4^o and 42.9^o were also obtained. The radiation properties of the 2×1 and 2×2 MIMO antennas at 3.6 GHz is presented in Figure 19 from where main lobe magnitudes of 7.51 dBi, and 7.48 dBi, main lobe directions of 8^o, and 4^o and HPBW of 73.3^o, and 69.5^o are observed. These results indicate good performance of the simulated antennas with nearly an omnidirectional radiation pattern and side lobe levels of -14.8 dB, and –15.3 dB is observed on average across all antennas.

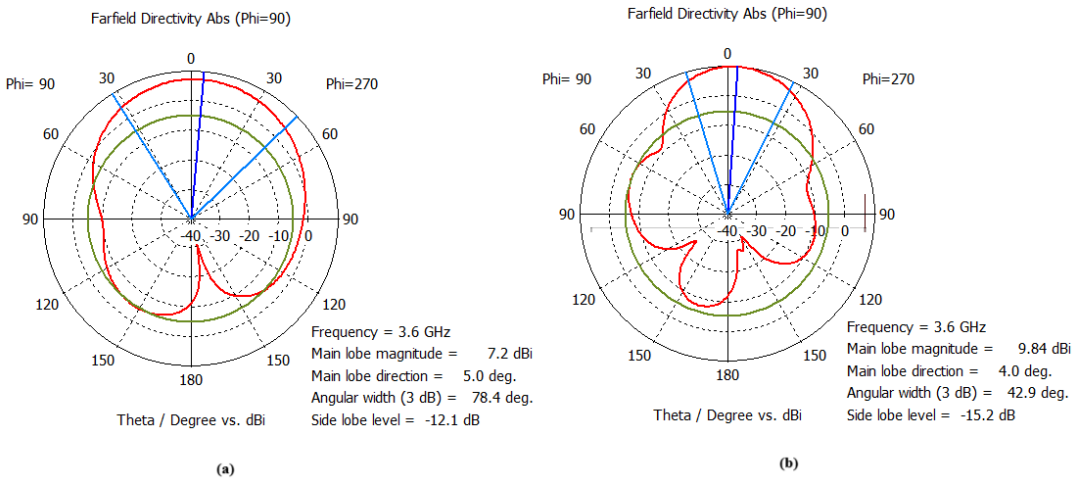

Figure 18: Antenna directivity at 3.6 GHz in H-plane ($\varphi = 90°$) (a) QWT-fed single patch (b) 2x1 series-fed patch

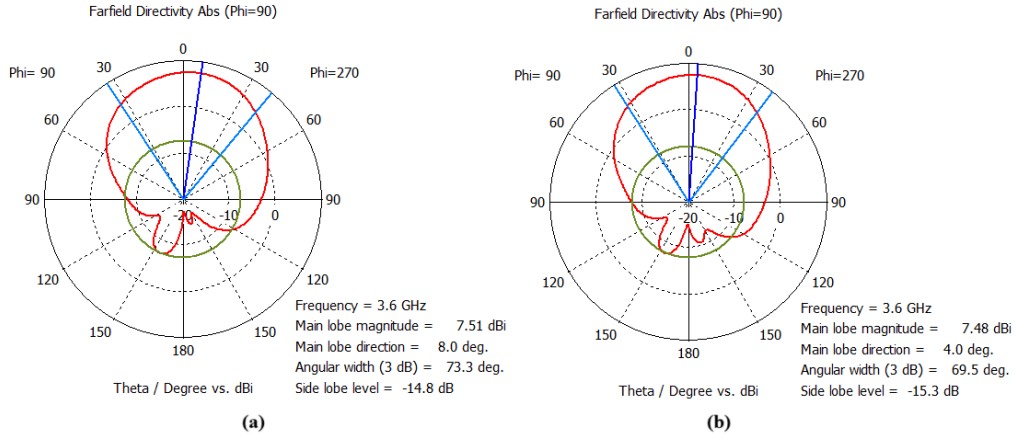

Figure 19: Antenna directivity at 3.6 GHz in H-plane (φ = 90°) (a) 2x1 MIMO antenna (b) 2x2 MIMO antenna

Figure 20 presents the directivity plot of the first element of both 40-element and 84-element mMIMO antennas where main lobe magnitudes of 7.51 dBi, and 9.91 dBi, main lobe directions of 5^o, and 1^o and HPBW of 71.4^o, and 41^o are observed.

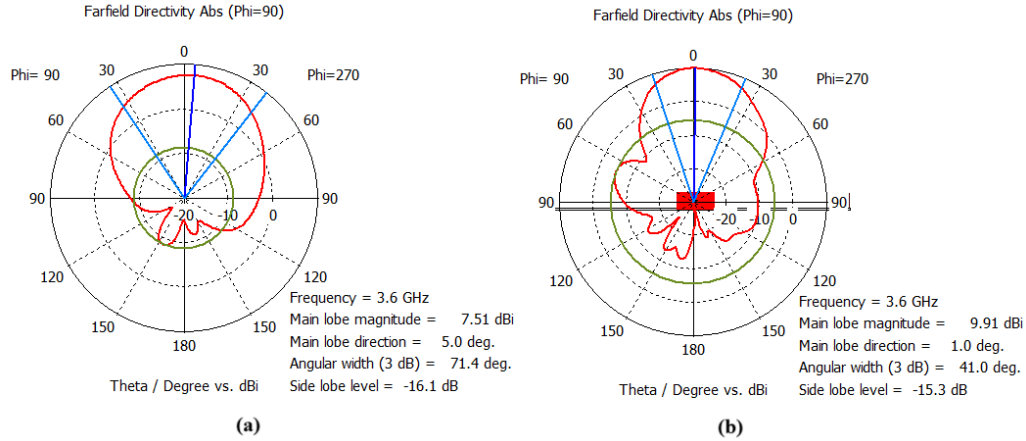

Figure 20: Antenna directivity at 3.6 GHz in H-plane (φ = 90°) (a) 40-element MIMO antenna (b) 84-element mMIMO antenna

The E-plane (φ = 0°) directivity of the QWT-fed single-element antenna and 2 × 1 series-fed antenna presented in Figure 21 shows similar performance to what was observed in the H-plane but with more reduced sidelobes.

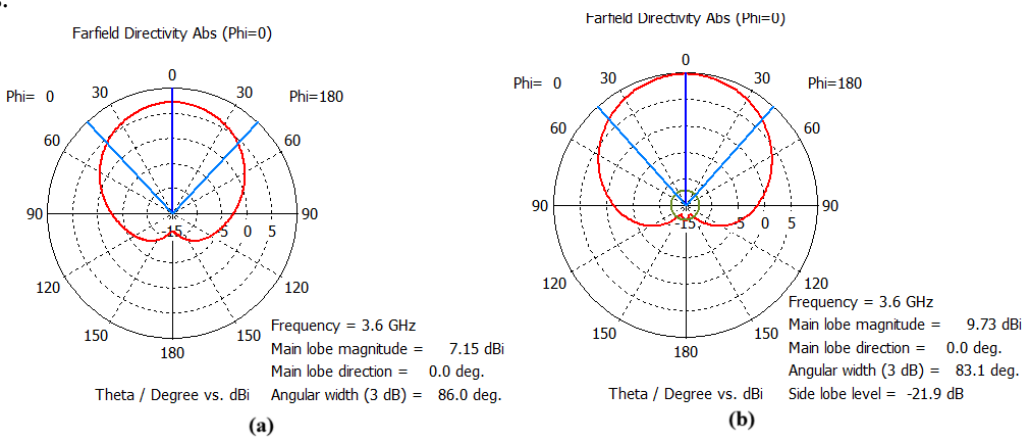

Figure 21: Antenna directivity at 3.6 GHz in E-plane (φ = 0°) (a) QWT-fed single patch (b) 2x1 series-fed patch

Figures 22 and 23 give the E-plane (φ = 0°) directivity of the 2 × 1 and 2 × 2 MIMO antennas. From Figure 22, main lobe magnitudes of 7.37 dBi and 7.46 dBi, the main lobe directions of 0^o, and 5^o and HPBW of 88^o, and 88.2^o, respectively. Main lobe magnitudes of 7.46 dBi and 9.91 dBi, main lobe directions of 4^o, and 2^o as well as HPBW of 88^o, and 88.2^o were achieved by the 40-element MIMO and 84-element mMIMO antennas, respectively, as presented in Figure 23.

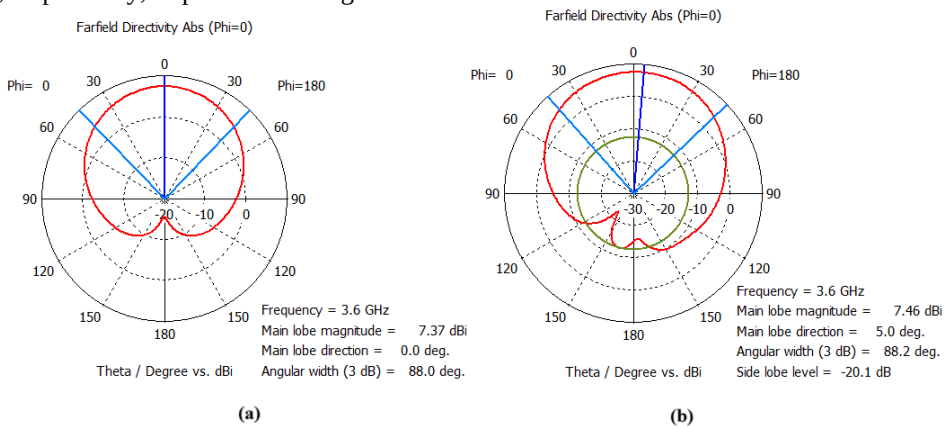

(a) (b)

Figure 22: Antenna directivity at 3.6 GHz in E-plane (φ = 0°) (a) 2x1 MIMO antenna (b) 2x2 MIMO antenna

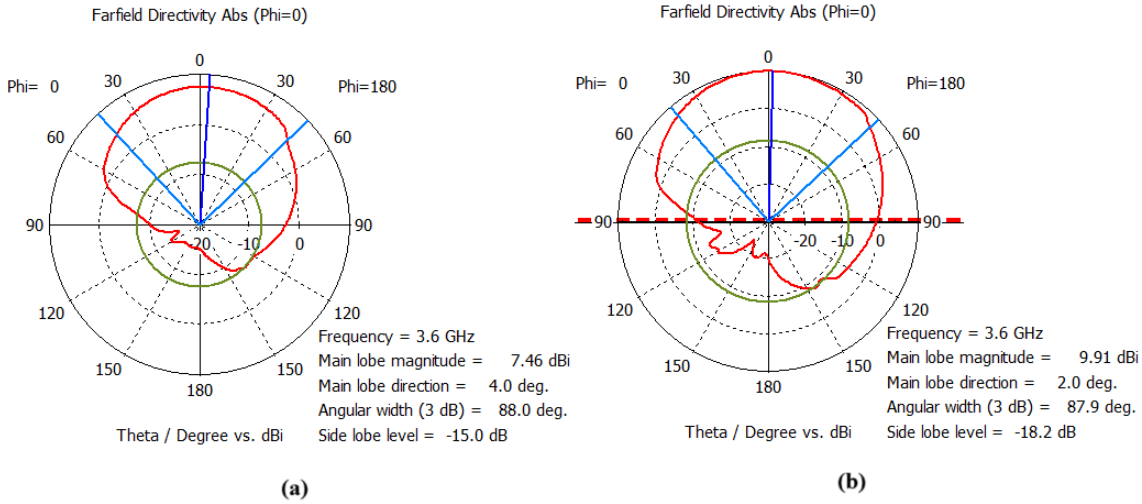

(a) (b)

Figure 23: Antenna directivity at 3.6 GHz in E-plane (φ = 0°) (a) 40-element MIMO antenna (b) 84-element mMIMO antenna

The results obtained and presented in this section highlighted the simulated output characteristics of MIMO and mMIMO antennas designed in Section 3. Bandwidths of 62.71 MHz, 72.33 MHz (and 67.81 GHz), 60.77 MHz, and 80.50 MHz were achieved by the QWT-fed single patch, 2x1 QWT-fed MIMO, 2x2 MIMO, and 2x1 series-fed antennas at 3.6 GHz respectively.

Natural isolation techniques (wide inter-element spacing) that inadvertently introduced spatial and polarisation diversity (cross-polarisation achieved through alternate antenna element arrangement) were adopted. The S-parameters of single patch and MIMO antennas presented in Figures 8 to 13 showed resonation within the allowable standard of $-10\ dB$ and $1 \leq VSWR \leq 2$. Also, matching reflection coefficients (S_{nn}) was observed on all MIMO antennas to be the same at the resonance frequency of 3.6 GHz; the converse is also true for S_{nm} plots. This was mainly due to the similarity of the antenna elements used in both cases of QWT and series feeding method.

Broadside radiation pattern was noticed from every directivity plot (polar plot) presented in the E- and H-plane (Figures 18 to 23) for both the single band antennas and the MIMO antennas. However, the proposed MIMO antennas achieved better signal directivity in both planes compared to the single-band antennas. Further analysis of the antennas showed appreciable diversity gain performance from computation and graphical representation. The calculation used the complex correlation coefficient value obtained from Figure 16. The

calculated ECC value (0.00002953) was far below the benchmark value of 0.5, with the DG computed value consistently maintaining a value of 9.99985 on the average across proposed MIMO antennas.

The gain achieved by all designed antennas for the QWT-fed antennas were above 6 dB and 9 dB by the series-fed antennas, as seen in Table 3. At the frequency of interest, mutual coupling was minimal, with an average port-to-port isolation of -21 dB.

The antenna proposed by Al-Ajrawi and Rahhal (2015) achieved a peak antenna gain of 8.35 dB (2x33 massive MIMO antenna), while the proposed 84-element mMIMO antenna achieved a gain of 9.38 dB at 3.6 GHz. The measured gain of the single port by Al-Tarifi et al. (2018) was 9.41 dB, which is in consonance with the proposed mMIMO antenna. Sandi et al. (2022) achieved an overall gain of 24.7 dB with their DRA-EBG-DGS antenna, which was higher than that the proposed mMIMO antenna achieved, and Nithya et al. (2021) were silent on their achieved gain; therefore, achieved gain comparison is not feasible with the proposed antenna.

V. CONCLUSION

In this paper, six (6) antennas – two single-band RMSAs (QWT- and 2×1 series-fed antenna), a 2×1, 2×2 and 40-element MIMO antenna and an 84-element massive MIMO antenna – have been designed, simulated and analysed. Clarifications have been given on parameters such as return loss, impedance bandwidth, gain, directivity, and VSWR, as well as ECC and DG for MIMO antennas in the six cases. From simulation results, with VSWR within specified limits, an average antenna gain of 6 dB for QWT-fed antennas (9 dB for the case of the series-fed antennas) and DG of 9.99985, the study's objectives have been realised. Also, a comparison of the proposed antennas was made with some of the reviewed works, with highlights showing that the antennas studied in this paper had superior port isolation, ECC and DG.

REFERENCES

[1]. Abedian, M., Rahim, S. K. A., Fumeaux, C., Danesh, S., Lo, Y. C., and Jamaluddin, M. H. (2017). Compact ultrawideband MIMO dielectric resonator antennas with WLAN band rejection. *IET Microwaves, Antennas and Propagation*, *11*:11, 1524–1529.

[2]. Aduke, A. A., Akaninyene, B. O., & Udofia, U. M. (2018). Compact dual-band triangular microstrip antenna with broadband characteristics for WLAN applications. *International Journal of Science and Engineering*, *7*:79, 132–136.

[3]. Al-Ajrawi, Y., & Rahhal, J. (2015). A simple antenna design for massive MIMO techniques. *2015 JIEEEC 9th Jordanian International Electrical and Electronics Engineering Conference, JIEEEC 2015*. https://doi.org/10.1109/JIEEEC.2015.7470743

[4]. Al-Tarifi, M. A., Sharawi, M. S., & Shamim, A. (2018). Massive MIMO antenna system for 5G base stations with directive ports and switched beamsteering capabilities. *IET Microwaves, Antennas and Propagation*, *12*(10), 1709–1718. https://doi.org/10.1049/iet-map.2018.0005

[5]. Amin, F., Saleem, R., Shabbir, T., ur Rehman, S., Bilal, M., & Shafique, M. F. (2019). A compact quad-element UWB-MIMO antenna system with parasitic decoupling mechanism. Applied Sciences (Switzerland), 9(11). https://doi.org/10.3390/app9112371

[6]. Balanis, C. A. (2016). Antenna Theory, Analysis and Design. (3rd ed.). John Wiley & Sons.

[7]. Bhatia, S., & Kunte, A. (2019). Exhaustive Appraisal of Adaptive Hybrid LTE-A Downlink Scheduling Algorithm. International Journal of Engineering and Advanced Technology (IJEAT), 9:2, 4765–4772. https://doi.org/10.35940/ijeat.B2632.129219

[8]. Chen, X., Zhang, S., and Li, Q. (2018). A Review of Mutual Coupling in MIMO Systems. *IEEE Access*, *6*, 24706–24719. https://doi.org/10.1109/ACCESS.2018.2830653

[9]. Dkiouak, A., Zakriti, A., Ouahabi, M. El, Touhami, N. A., & Mchbal, A. (2019). Design of a four-element MIMO antenna with low mutual coupling in a small size for satellite applications. Progress In Electromagnetics Research M, 85(September), 95–104. https://doi.org/10.2528/pierm19071202

[10]. Garg, R., Bhartia, P., Bahl, I., and Ittipiboon, A. (2001). Microstrip Antenna Design Handbook. Artech House.

[11]. Huang, Y., and Boyle, K. (2008). Antennas From Theory to Practice (1st ed.). John Wiley & Sons.

[12]. Jamshed, M. A., Ur-Rehman, M., Frnda, J., Althuwayb, A. A., Nauman, A., and Cengiz, K. (2021). Dual Band and Dual Diversity Four-Element MIMO Dipole for 5G Handsets. Sensors, 1–13.

[13]. Kim, G., and Kim, S. (2021). Design and Analysis of Dual Polarized Broadband Microstrip Patch Antenna for 5G mmWave Antenna Module on FR4 Substrate. IEEE Access, 9, 64306–64316. https://doi.org/10.1109/ACCESS.2021.3075495

[14]. Kuboye, B. M. (2018). Performance Evaluation of Scheduling Algorithms for 4G (LTE). Communications and Network, 10, 152–163. https://doi.org/10.4236/cn.2018.104013

[15]. Kumar, A., and Gupta, R. (2013). Genetic Algorithm in Broadband Microstrip Antenna design. International Journal of Advanced Research in Computer and Communication Engineering, 2(3), 1469–1472.

[16]. Kumar, G., and Ray, K. P. (2003). Broadband microstrip antennas. Artech House.

[17]. Li, M. Y., Ban, Y. L., Xu, Z. Q., Guo, J., and Yu, Z. F. (2018). Tri-Polarized 12-Antenna MIMO Array for Future 5G Smartphone Applications. IEEE Access, 6(December), 6160–6170. https://doi.org/10.1109/ACCESS.2017.2781705

[18]. Nithya, S., Sandhiya, M., Sathish Kumar, R., Vaishnavi, S., and Vishnu Prasad, S. R. (2021). Design and Fabrication of Microstrip MIMO Antenna for 5G Smart Phones. Journal of Physics: Conference Series, 1916(1). https://doi.org/10.1088/1742-6596/1916/1/012199

[19]. Sandi, E., Diamah, A., and Al Mawaddah, M. (2022). High isolation MIMO antenna for 5G C-band application by using combination of dielectric resonator, electromagnetic bandgap, and defected ground structure. Eurasip Journal on Wireless Communications and Networking, 2022(1), 1–13. https://doi.org/10.1186/S13638-022-02208-1/TABLES/5

[20]. Saturday, J. C., Udofi, K. M., and Obot, A. B. (2017). Compact Rectangular Slot Patch Antenna for Dual Frequency Operation Using Inset Feed Technique. International Journal of Information and Communication Sciences, 1(3), 47–53. https://doi.org/10.11648/j.ijics.20160103.13

[21]. Saurabh, A. K., Rathore, P. S., and Meshram, M. K. (2020). Compact wideband four-element MIMO antenna with high isolation. Electronics Letters, 56(3), 117–119. https://doi.org/10.1049/el.2019.2871

[22]. Singh, K. K., and Gupta, S. C. (2013). Review and Analysis of Microstrip Patch Array Antenna with different configurations. International Journal of Scientific & Engineering Research, 4(2), 1–6.

[23]. Wang, Q., Mu, N., Wang, L., Safavi-Naeini, S., and Liu, J. (2017). 5G MIMO Conformal Microstrip Antenna Design. Wireless Communications and Mobile Computing, 2017. https://doi.org/10.1155/2017/7616825

[24]. Yang, R., Xi, S., Cai, Q., Chen, Z., Wang, et al. (2021). A compact planar dual- band multiple- input and multiple- output antenna with high isolation for 5g and 4g applications. Micromachines, 12:5, 2–9. https://doi.org/10.3390/mi12050544

[25]. Yussuff, A. I., and Khamis, N. H. (2012). Rain Attenuation Modelling and Mitigation in The Tropics: Brief Review. International Journal of Electrical and Computer Engineering (IJECE), 2(6), 748–757. https://doi.org/10.11591/ijece.v2i6.1222

[26]. Zhao, A., Member, S., and Ren, Z. (2019). Size Reduction of Self-Isolated MIMO Antenna System for 5G Mobile Phone Applications. IEEE Antennas and Propagation Letters, 18:1, 152–156.